AIP | Applied Physics Letters

Underwater depth reconstruction by local water wave measurements

A. Przadka, P. Petitjeans, V. Pagneux, A. Maurel, and R. K. Ing

Citation: Appl. Phys. Lett. **103**, 144105 (2013); doi: 10.1063/1.4823529
View online: http://dx.doi.org/10.1063/1.4823529
View Table of Contents: http://apl.aip.org/resource/1/APPLAB/v103/i14
Published by the AIP Publishing LLC.

Underwater depth reconstruction by local water wave measurements

A. Przadka,[1] P. Petitjeans,[1] V. Pagneux,[2] A. Maurel,[3] and R. K. Ing[3]
[1]*Physique et Mécanique des Milieux Hétérogènes, PMMH, UMR CNRS 7636-ESPCI-UPMC Université Paris 6-UPD Université Paris 7, Paris, France*
[2]*Laboratoire d'Acoustique de l'Université du Maine, UMR CNRS 6613, Avenue Olivier Messiaen, 72085 Le Mans, France*
[3]*Institut Langevin, UMR CNRS 7587-UPD Université Paris 7, 1 rue Jussieu, 75238 Paris, France*

(Received 21 March 2013; accepted 9 September 2013; published online 1 October 2013)

We present an experimental study of underwater depth reconstruction obtained by a method based on the Bessel series expansion of the solutions of the 2D linear water wave equation. This is achieved by measuring capillary-gravity waves using a contactless space-time resolved Fourier Transform Profilometry method. The ability of the method is exemplified for several type of bathymetry in laboratory experiments. © *2013 AIP Publishing LLC*. [http://dx.doi.org/10.1063/1.4823529]

The bathymetry of shallow water areas is of particular interest for coastal engineering. Among the available techniques, conventional sea floor surveying by single and multibeam echo sounders is slow and covers only around 10% of ocean surface.[1,2] Airborne Lidar Bathymetry (ALB) systems, that survey shallow continental waters, remain limited on the maximum detectable depth.[3–6] In the extreme cases of high turbidity and/or poor reflectance, the ALB measurements cannot be performed.

This letter introduces an approach to water depth reconstruction which requires only the surface wave elevation information. It is based on basic properties of the solution to finite depth water wave equation; this so called circle method benefits from the Bessel series expansion of the solutions of the 2D linear wave equation (already used to study thickness and velocity of plates[7,8]). The theoretical description of the problem is presented and the ability of the bottom shape characterization is demonstrated experimentally.

Let us consider wave propagating on the water surface with wavenumber k linked to the pulsation ω by the linear dispersion relation[9]

$$\omega^2 = \left(gk + \frac{\gamma}{\rho}k^3\right)\tanh(kH), \tag{1}$$

where g denotes the gravity acceleration, ρ the water density, γ the surface tension, and H the water depth. Note that in general $k(\omega)$ is a complex number where the real part is related to the wavelength and the imaginary part describes the attenuation. In an area of constant water depth, the surface elevation perturbation is a solution of the 2D Helmholtz equation

$$(\Delta + k^2(\omega))\hat{\eta} = 0. \tag{2}$$

In the above equation, $\hat{\eta}$ stands for the time Fourier transform of the measured transient height $\eta(\mathbf{x}, t)$

$$\hat{\eta}(\mathbf{x}, \omega) = \int_{-\infty}^{\infty} \eta(\mathbf{x}, t)e^{-i\omega t}dt. \tag{3}$$

Equation (1) shows that the wavenumber depends on the water depth H as long as $\tanh(kH)$ is not too close to 1. This regime corresponds to the finite depth regime where the wave feels the water bottom, i.e., for a fixed frequency, the wavelength λ depends on the water depth H as long as $\lambda \gtrsim H$. This property will be used to obtain the local depth H through local measurements of the wavenumber k.

Let us consider a circle of radius R (Fig. 1) inside an area of constant depth H. Inside the circle, the surface elevation η—solution to the Helmholtz equation (2)—can be expressed in polar coordinates as

$$\hat{\eta}(r, \theta, \omega) = \sum_{n=-\infty}^{n=+\infty} a_n J_n(kr)e^{in\theta}, \tag{4}$$

where $r \leq R$ is the radial coordinate and θ is the polar angle. For the circle method, we will use two properties of this solution (4). Firstly, the average value of the surface elevation on the circle is defined as

$$\langle\eta\rangle_R = \frac{1}{2\pi}\int_{C_R} \hat{\eta}(R, \theta, \omega)d\theta = a_0 J_0(kR). \tag{5}$$

Secondly, the value of the surface elevation at the center of the circle is given by $\eta(0) = a_0$. Consequently, the ratio of the average value of the surface elevation on the circle to the value at the center is

$$\frac{\langle\eta\rangle_R}{\eta(0)} = J_0(k(\omega)R). \tag{6}$$

This formula forms the basis of the method: the wavenumber k is obtained from the measurements of the surface elevation at the center and on the circle of known radius R.

Experimentally, the surface elevation $\eta(x, y, t)$ is measured for a broadband excitation signal. Fourier Transform is performed to get $\hat{\eta}$, and the signal ratio $\langle\eta\rangle_R/\eta(0)$ is obtained as a function of the frequency ω. This gives us the dispersion function $k(\omega)$ over a broad range of frequencies. Then, this curve $k(\omega)$ is fitted using the theoretical dispersion relation $k_{theory}(\omega, H)$ in Eq. (1) to get the H-value that minimizes $|k - k_{theory}|$ over the entire range of frequency. This makes the method more accurate and more robust than the use of a unique value k at a unique frequency.

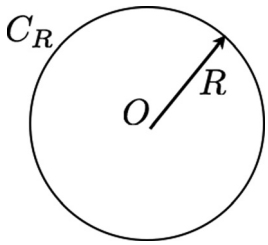

FIG. 1. Geometry of the circle.

The experiments have been carried out in the tank with dimensions 53 × 38 cm^2 filled with water with an attenuation that has been characterized[10] and varying depth $H(x,y)$. The surface elevation $\eta(x,y,t)$ was measured with a good accuracy in time and in space during the wave propagation using the optical Fourier Transform Profilometry (FTP) method. This method is based on the analysis of the deformation of projected fringes[10–12] and uses a Photron SA4 high-speed video camera of 125 frames rate per second to image the surface. This method enables space-time resolved measurements of water waves and is particularly well suited to characterize non-stationary phenomena.[13–15]

In the experiment, the transient waves are produced by a conical vibrator that can be considered as a source point. A one-period sinusoidal pulse centered at $f_0 = 4$ Hz was chosen exciting a wave packet of broadband frequencies. The perturbation $\eta(x,y,t)$ is measured during 50 s till the total attenuation of the wave. To calculate the averaged value of the surface elevation along a circular path, N positions regularly distributed along the circle are chosen and signals at these points are linearly interpolated from data of the FTP device and then averaged. In general, N is chosen big enough to have an averaged surface elevation signal close to that really measured along a circle. Results shown in this letter are achieved using $N = 90$. Three different geometrical configurations have been studied:

- C1: basin with constant liquid depth $H_0 = 12$ mm.
- C2: a conical, step pyramid is placed in the middle of the bottom of the configuration C1. The geometry of the pyramid is shown in Fig. 2. The total pyramid height is 10 mm, thus is 2 mm below the liquid free surface.
- C3: different objects of different heights are immerged inside the basin of $H_0 = 47$ mm liquid depth (Fig. 6(a)).

The first geometrical configuration C1 with constant depth was used to characterize accuracy level and resolution of the circle method for water waves. The wavelength λ_0 corresponding to the central frequency f_0 for $H_0 = 12$ mm is equal to 80 mm and water can be treated as shallow. Fig. 3 shows the real part of the signal ratio as a function of the product kR for different values of R. It can be observed that kR variations fit well Bessel function even for low values of R. For these values however, the fitting process is not expected to be accurate, because the Bessel curve is not well enough defined. Therefore, a biased value of the liquid depth H parameter is expected. The used frequency bandwidth is 0.1 Hz–5.5 Hz.

Fig. 4 shows variation of the liquid depth parameter H (after fitting process) versus radius circle R. The fitting process is based on the minimization of the quadratic error. It is observed that H parameter evolves toward an asymptotic value. The final value to within 5% is reached when the radius R is greater than 10 mm. At 5.5 Hz, the surface elevation wavelength λ_{min} is equal to 52 mm. The final value to within 5% is achieved when the circle radius is approximately higher than $\lambda_{min}/4$.

Since the depth of the liquid without obstacles H_0 is known for each configuration, we can introduce a value $s(x,y)$, which stands for a local shape of the bottom (bathymetric map) and can be calculated as the difference between known liquid depth without obstacles H_0 and locally obtained liquid depth H

$$s(x,y) = H_0 - H(x,y). \tag{7}$$

In the case of configuration C2, Fig. 5 represents the bathymetric maps computed with two different radii $R = 10$ mm and $R = 20$ mm. As expected, for low values of R, the liquid depth values are biased and weaker H values are obtained. In this case, resolution is however better. For larger values of

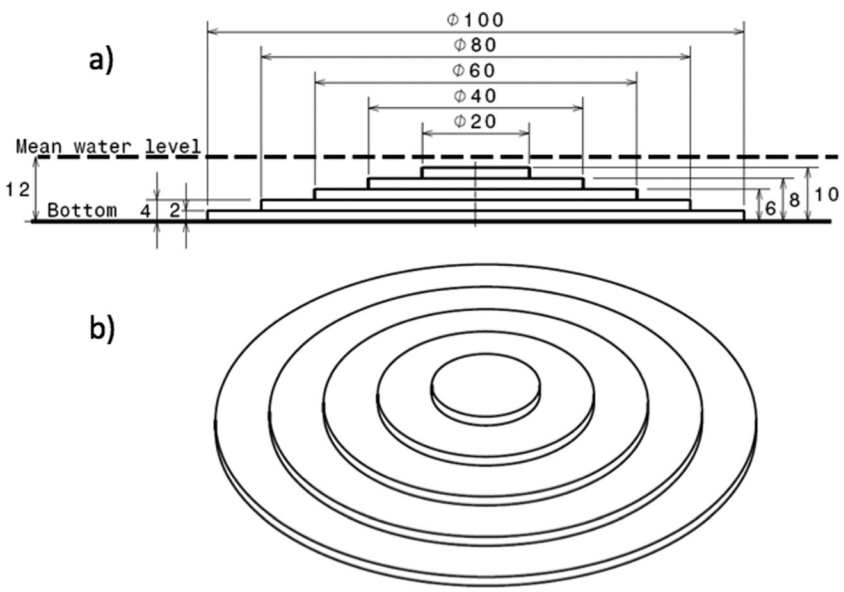

FIG. 2. Geometrical configuration C2: side view with dimensions (a) and a 3D view (b).

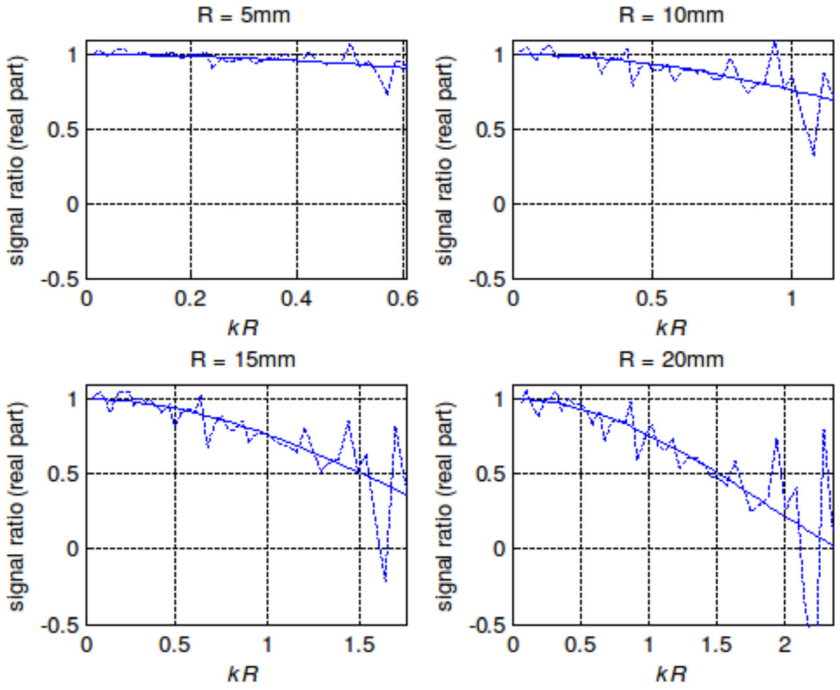

FIG. 3. Signal ratio $\langle\eta\rangle_R/\eta(0)$ versus kR for different values of R. Dotted lines: experimental data. Solid lines: Bessel J_0 fitting function.

R, the liquid depth value is more accurate especially in areas of constant value, but the conical pyramid is well less defined. In the neighbourhood of the obstacle, constant bottom was found to be deeper than in reality.

In configuration C3 several objects are immersed inside the basin. The geometrical configuration is shown in Fig. 6(a). Each value shown on the top of each object corresponds to its height. The liquid level in the basin is $H_0 = 47$ mm.

Experimentally determined bottom shape $s(x,y)$ distribution is presented in Fig. 6(b). All the obstacles (except the one with lowest height) are reconstructed by the method. The obstacles are found to be broader than in reality because of the influence of the radius R. The bottom of the tank is in agreement with the theory. The obstacle with lowest height (3 mm) cannot be found due to the small deviation in the Bessel function between the depth of the liquid over the bottom of the tank and over the obstacle. Cylinders with height 25 mm and 30 mm can be observed, but the reconstructed height values are around 20% lower than the real values. The black cylindrical obstacle—even high enough to be correctly detected—has small diameter and due to the circle radius R influence its height is found to be lower than its real value. Positions and heights of other obstacles are correctly determined.

The present work shows a method for bathymetry characterization using the analysis of finite depth water waves. Compared with conventional techniques using beam echo sounders, our method is not limited by the minimum depth in which ships can operate. However, it is limited in terms of

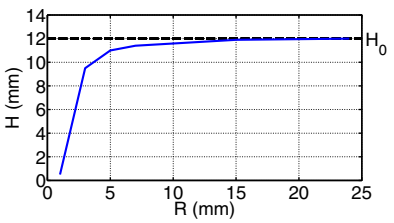

FIG. 4. Liquid depth H versus circle radius R.

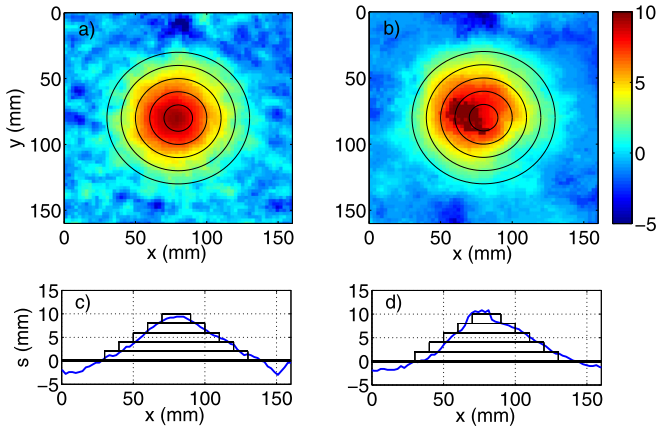

FIG. 5. Bathymetric maps $s(x,y)$ obtained experimentally for two different values of $R = 10$ mm (a) and $R = 20$ mm (b). (c) and (d) shows bottom shape for a horizontal cut at $y = 80$ mm.

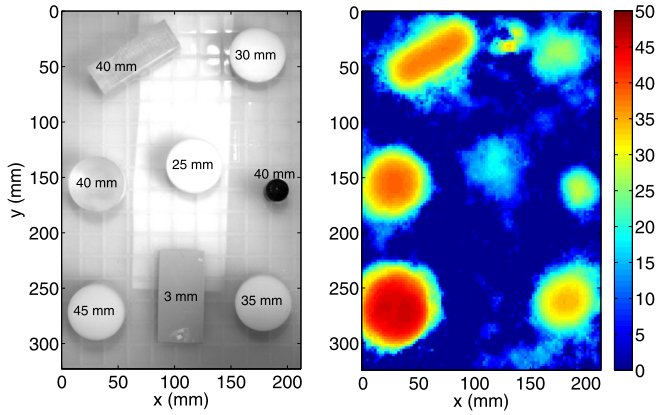

FIG. 6. Configuration C3: geometry of the bottom (left) and corresponding bathymetric maps (right) obtained experimentally by means of the circular method ($R = 20$ mm) for liquid depth $H_0 = 47$ mm. The color scale of the local bottom shape $s(x,y)$ is given in millimeters.

maximum detectable depths. This is because the depth cannot be much larger than the wavelengths of the water waves. Note that a maximum detectable depth exists also for the Airborne Lidar Bathymetry which is around 60 m in very good conditions and depends on the water clarity and bottom reflectance.

The assumption is that the wave obeys the wave equation in linear regime. Experimental measurements are achieved using waves of weak steepness to ensure such an assumption. In reality, non linear conversions should occur when the surface wave propagates over submerged breakwaters.[16] Extensive studies will be conducted on this subject later. In the vicinity of the steep obstacle evanescent waves and vortex shedding could occur. These physical phenomena are not taken into account in the circle method and this might bias results by making false the geometrical dimension of the obstacle in addition to the smoothing effect due to the circular integration of the surface waves. Another assumption is that the depth is locally constant. Experiments show the validity of the method and its efficiency for depth varying slowly over a distance of one wavelength. The liquid depth is determined locally except in the vicinity (typically the order of the wavelength) of depth discontinuities. The method is robust and weakly sensitive to noise since it is based on integration of the wave dynamics over a broad range of frequencies and a circular path in space.

A.M., V.P., A.P. and P.P. acknowledge the financial support of the Agence Nationale de la Recherche through the grant DYNAMONDE ANR-12-BS09-0027-01

[1]J. J. Becker, D. T. Sandwell, W. H. F. Smith, J. Braud, B. Binder, J. Depner, D. Fabre, J. Factor, S. Ingalls, S. H. Kim, R. Ladner, K. Marks, S. Nelson, A. Pharaoh, R. Trimmer, J. Von Rosenberg, G. Wallace, and P. Weatherall, Mar. Geodesy **32**(4), 355–371 (2009).
[2]W. H. F. Smith and D. T. Sandwell, Science **277**, 1956–1962 (1997).
[3]S. Pe'eri, L. V. Morgan, W. D. Philpot, and A. A. Armstrong, J. Coastal Research **62**, 75–85 (2011).
[4]T. Allouis, J.-S. Bailly, Y. Pastol, and C. Le Roux, Earth Surf. Processes Landforms **35**, 640–650 (2010).
[5]S. Mitchell, J. P. Thayer, and M. Hayman, Appl. Opt. **49**(26), 6995–7000 (2010).
[6]G. C. Guenther, A. G. Cunningham, P. E. LaRocque, and D. J. Reid, in *Proceedings of the 20th EARSeL Symposium: Workshop on Lidar Remote Sensing of Land and Sea, European Association of Remote Sensing Laboratories, Dresden, Germany, 16–17 June 2000* (EARSeL eProceeding, 2000), p. 28.
[7]R. K. Ing, N. Etaix, A. Leblanc, and M. Fink, J. Acoust. Soc. Am. **127**(6), EL252–EL257 (2010).
[8]N. Etaix, A. Leblanc, M. Fink, and R. K. Ing, IEEE Trans. Ultrason. Ferroelectr. Freq. Control **57**(8), 1804–1812 (2010).
[9]L. D. Landau and E. M. Lifshitz, *Fluid Mechanics* (Pergamon, New York, 1959).
[10]A. Przadka, B. Cabane, V. Pagneux, A. Maurel, and P. Petitjeans, Exp. Fluids **52**(2), 519–527 (2012).
[11]P. Cobelli, A. Maurel, V. Pagneux, and P. Petitjeans, Exp. Fluids **46**, 1037–1047 (2009).
[12]A. Maurel, P. Cobelli, V. Pagneux, and P. Petitjeans, Appl. Opt. **48**(2), 380–392 (2009).
[13]P. Cobelli, V. Pagneux, A. Maurel, and P. Petitjeans, Europhys. Lett. **88**, 20006 (2009).
[14]P. Cobelli, A. Przadka, P. Petitjeans, G. Lagubeau, V. Pagneux, and A. Maurel, Phys. Rev. Lett. **107**, 214503 (2011).
[15]G. Lagubeau, M. A. Fontelos, C. Josserand, A. Maurel, V. Pagneux, and P. Petitjeans, Phys. Rev. Lett. **105**, 184503 (2010).
[16]M. Christou, C. Swan, and O. T. Gudmestad, Coastal Eng. **55**, 945–958 (2008).